

Prediction of virus survival timescales in surrogate respiratory sessile droplets

Cite as: Phys. Fluids **35**, 057109 (2023); doi: [10.1063/5.0143813](https://doi.org/10.1063/5.0143813)

Submitted: 26 January 2023 · Accepted: 22 April 2023 ·

Published Online: 5 May 2023








View Online



Export Citation



CrossMark

Cosimo Brondi,¹  Nicolò G. Di Novo,¹  Nicola M. Pugno,^{1,2}  Giuseppe Mensitieri,^{3,a)} 
and Massimiliano Fraldi^{4,a)} 

AFFILIATIONS

¹Laboratory for Bioinspired, Bionic, Nano, Meta Materials and Mechanics, Department of Civil, Environmental and Mechanical Engineering, University di Trento, 38123 Trento, Italy

²School of Engineering and Materials Science, Queen Mary University of London, E1 4NS London, United Kingdom

³Department of Chemical, Materials and Production Engineering, University of Napoli Federico II, 80125 Napoli, Italy

⁴Department of Structures for Engineering and Architecture, University of Napoli Federico II, 80125 Napoli, Italy

Note: This paper is part of the special topic, Flow and the Virus.

a) Authors to whom correspondence should be addressed: mensitie@unina.it and fraldi@unina.it

ABSTRACT

The spreading of respiratory diseases through deposited saliva droplets is strongly dependent on the water evaporation process that may determine the virus viability due to the increase in concentration of nonvolatile compounds that are harmful for the virus. The drying time of a virus-laden droplet is influenced by environmental conditions, such as relative humidity and temperature, physical properties, such as the features of the surface on which it is deposited, and the wetting regime. Under this perspective, we addressed the modeling of an evaporating sessile droplet resting on a flat smooth surface, extending a previous diffusion-based model from the same authors. The evaporation behavior of sessile droplets of aqueous sodium chloride solutions and the virus viability of a surrogate virus (MS2) have been simulated considering different wetting regimes to account for different types of surfaces, ranging from highly hydrophilic to highly hydrophobic, as well as different ambient conditions, in terms of temperature and relative humidity. The results of calculations were given in terms of time evolution of contact angle, contact radius, mixture volume, and salt concentration, unveiling the importance of different wetting regimes for evaporation behavior and drying time. Longer evaporation times have been observed as temperature decreases and relative humidity increases. With reference to a surrogate virus, we evaluated the virus viability at different selected conditions, observing the classical U-shape of relative viability as a function of relative humidity of the environment at a certain temperature.

Published under an exclusive license by AIP Publishing. <https://doi.org/10.1063/5.0143813>

I. INTRODUCTION

Pandemic diseases are a threat of great concern in the twenty-first century, as is the one caused by the well-known SARS-CoV-2 (Severe Acute Respiratory Syndrome Coronavirus 2) that already took lives of millions of people. The rapid spread of SARS-CoV-2 raised important questions regarding the transmission mechanisms and the role potentially played by airborne transmission, indicating that for this virus the contamination is primarily caused by virus inhalation.¹

Several works have been devoted to elucidating the spreading mechanism of viruses, reporting that virulent diseases may be transmitted via aerosols, which remain suspended in air long enough to be inhaled, or droplets that may either directly affect a susceptible person or get deposited on a substrate before being transferred from a surface

to a human body.^{2,3} As a matter of fact, enveloped and non-enveloped viruses may survive inside expectorated respiratory droplets deposited on surfaces for several days.⁴

With reference to a sessile droplet placed on a flat substrate, the key parameters ruling the evaporation process and the time needed for total or partial evaporation of the droplet are the type of surface and its interaction with the droplet, e.g., substrates with different thermal properties,^{5,6} surface topography,^{7,8} and chemical affinity between the substrate and the droplet;^{9,10} the types of different solutes present within the droplet and their concentration;^{11,12} the wetting regime, e.g., total or partial spreading of the droplet on the surface;¹³ and, finally, the environmental conditions, e.g., the relative humidity (RH) and the temperature.^{14–16} Under this perspective, it is important to assess which are the parameters that regulate the evaporation process

to properly design new surfaces with the purpose of frustrating the viability of viruses carried by the droplets.

In this regard, ambient humidity and temperature severely affect virus viability in biological fluids. In fact, it has been reported that some enveloped viruses,^{17–20} included in respiratory aerosol as well as in deposited droplets, are characterized by the so-called U-shape behavior. Starting from very high values of *relative humidity* (*RH*), the viral load displays a high viability that decreases as *RH* decreases reaching a minimum value at intermediate *RH*s and then increases again up to high values as the *RH* still decreases ($RH \leq 50\%$). In this way, three regimes of viability in terms of *RH* can be identified.^{17,18} As a consequence, when aerosols or droplets are exhaled into the surrounding environment (containing unsaturated air, i.e., $RH < 100\%$), they may either fully or partially evaporate to allow the attainment, at the aerosol (or droplet) interface, of a water vapor pressure in equilibrium with ambient conditions.¹⁸

The respiratory droplet is a complex mixture of several solutes, such as salts and proteins, at variable concentration values that increase as water evaporation proceeds. This event influences in a dramatic way the microenvironment in which the viruses are embedded, affecting, therefore, their viability.²⁰

Lifetime of virus-laden droplets is also dependent on the wetting behavior and the type of substrate that is reflected in the dependency on the *contact angle* (*CA*) formed between the solid surface and the droplet. Bhardwaj and Agrawal²¹ modeled the evaporation of a pure water sessile droplet placed on a partially wetted surface with a pinned contact line (*CL*) and observed that the drying time was strongly affected by the droplet volume, *CA*, ambient temperature, and humidity. In a follow-up study,²² same authors observed that there is a drastic difference between the drying time of respiratory droplets and the survival time of the coronavirus on different surfaces (order of seconds vs order of hours, respectively), attributing this discrepancy in the timescales to a thin liquid film that remains after the evaporation of the initial sessile droplet. A further development has been reported by Kumar in Ref. 23, where the role of a *stick-slip* (*SS*) evaporation mode on the lifetime of COVID-19 droplets has been investigated on materials with a different wettability. However, despite the efforts made so far, the physics underlying these phenomena is not yet fully understood, and simple thermodynamic models capable of predicting and describing the above-mentioned regimes have not been wholly exploited.

To the best of our knowledge, most of the existing reports on the drying time of virus-laden droplets have been devoted only to the study of a *pinned contact line* mode (e.g., constant contact area) in terms of wetting behavior and with reference to pure liquids (e.g., water, usually assumed to behave like saliva droplets, which are characterized instead by a more complex composition²⁰). Starting from these recent achievements in the literature, we adopted a mathematical model of a spherical cap droplet located on a flat substrate. We essentially focused on two crucial points in developing our model: (i) the introduction of a simple relation (already introduced in Ref. 24 but only used for pure liquids) that allows a global analysis of the wetting regime on different substrates (e.g., from hydrophilic to hydrophobic surfaces) and (ii) the analysis of the evaporation process at different ambient temperatures. The points (i) and (ii) represent two major steps forward with reference to our previous work²⁵ and allow, with reference to the literature, the extension of the

evaporation model with these new implemented features from pure water systems to aqueous sodium chloride solutions.

We investigated the evaporation behavior, the wetting regime, and the compositional evolution of sessile droplets in terms of *CA*, *contact radius* (*CR*), *mixture volume*, and *salt concentration*. In this way, it was possible to analyze the dependence of the virus viability on the environmental conditions, such as *RH* and temperature (*T*, not investigated in Ref. 25), and on the material surface characteristics, through the initial *CA* (θ_0) and the receding *CA* (θ_R), by relating the evaporation of saline sessile droplets to a proper measure of the so-called *cumulative dose* (*CD*) of harmful compounds to which the virus is exposed inside the droplet. The interesting final finding of this work may provide insight about one of the key parameters ruling the interaction between the liquid droplet and the solid substrate, namely, the wetting behavior that occurs when a sessile droplet is resting on a flat smooth surface. However, it should be underlined that, in the current version of the model, the effect of the chemical nature of the solid substrate on the viability of viruses placed inside a sessile droplet standing on it has not been considered.

II. METHODS

A. Modeling the evaporation of a sessile droplet on a flat substrate

In this work, a widely used model^{24,26–28} of a sessile droplet of saliva is adopted, which consists of an aqueous solution of sodium chloride placed on a flat substrate. Important assumptions are that both the Bond number [$Bo = (\rho_{mix}^l g R^2)/\sigma_{mix}^l$, with ρ_{mix}^l and σ_{mix}^l being the density and the surface tension of the liquid mixture, respectively, g the acceleration of gravity, and R the contact radius] and the capillary number [$Ca = (\mu_{mix}^l u_r)/\sigma_{mix}^l$, with μ_{mix}^l and u_r being the viscosity of the liquid mixture and the characteristic flow velocity within the droplet, respectively] are much smaller than 1 during the whole evaporation process.²⁹ Therefore, the effect of the gravitational forces over the surface tension can be neglected, and the internal flows are too weak to alter the interface shape so that the droplet shape can be considered as a spherical cap,^{26,27}

$$V_{mix} = \pi R^3 g(\theta), \tag{1}$$

where θ and R , respectively, are the *CA* and the *CR*, and $g(\theta)$ has the following expression:

$$g(\theta) = \frac{\cos \theta^3 - 3 \cos \theta + 2}{3 \sin \theta^3}. \tag{2}$$

From Eqs. (1) and (2), we obtain the geometrical parameters (i.e., *CA*, *CR*, and V_{mix}). Based on this, the other parameter can be easily calculated. Accordingly, at the initial phase of the evaporation process, the initial contact radius R_0 can be derived from the known initial mixture volume V_{mix0} and initial contact angle θ_0 . Overall, from the geometric considerations, the volume evaporation rate dV_{mix}/dt can be expressed as a function of the time-derivatives of θ and R as follows :

$$\frac{dV_{mix}}{dt} = \frac{\pi R^3}{(1 + \cos \theta)^2} \frac{d\theta}{dt} + 3\pi R^2 g(\theta) \frac{dR}{dt}. \tag{3}$$

We also adopted the widely used hypothesis that the evaporation process is slow enough into the stagnant air so that the mass transfer is solely limited by the water diffusion within the gaseous phase

surrounding the droplet. This assumption is fulfilled when the characteristic time of diffusion is negligible with respect to the evaporation time [i.e., when $R^2/(D_w t_{ev}) \ll 1$, with D_w and t_{ev} being the water diffusivity in air and the evaporation time, respectively].^{26–28} Data related to the dependence of the water diffusion coefficient (m^2/s) on temperature T (K) were retrieved from Bhardwaj and Agrawal.^{21,22} In addition, the slow evaporation rate allows to assume inside the droplet the uniformity of the profile of temperature, which is equal to the environmental temperature T .^{24,26} In addition, the quasi-steady state assumption for the diffusion process allows a simple formulation of the mass balance of water vapor within the gaseous phase, reducing the problem to the solution of a Laplace equation in terms of water concentration ρ_w^v . With the above-mentioned assumptions, a formal solution in terms of instantaneous total mass evaporation rate was proposed by Popov²⁷ as follows:

$$\frac{dm_{mix}}{dt} = -\pi R D_w (\rho_w^{v,sat} - \rho_w^{v,\infty}) f(\theta), \quad (4)$$

where $\rho_w^{v,sat}$ and $\rho_w^{v,\infty}$ stand for the water vapor concentration in the surrounding air at the droplet–air interface and in the bulk of the air phase, respectively, while $f(\theta)$ is the function that encloses the dependence on the temporal evolution of the CA. The same author reported an analytical form for $f(\theta)$,^{26,27}

$$f(\theta) = \frac{\sin(\theta)}{1 + \cos(\theta)} + 4 \int_0^\infty \frac{1 + \cos h(2\theta\tau)}{\sin h(2\pi\tau)} \tan h[(\pi - \theta)\tau] d\tau. \quad (5)$$

However, Eq. (5) is not in a closed form and needs to be calculated by a numerical integration method. Among the several expressions proposed as an approximation of Eq. (5),^{24,26,27,30,31} Hu and Wu reported a closed-form expression of simple application that well fits the analytical form²⁴

$$f(\theta) = \frac{1}{\sqrt{1 + \cos(\theta)}}. \quad (6)$$

Equation (6) holds for $0 \leq \theta \leq 180^\circ$; thus, this analysis can cope with several types of substrates (e.g., $\theta_0 < 90^\circ$ for hydrophilic surfaces or $\theta_0 > 90^\circ$ for hydrophobic surfaces). If this approximation is used, the instantaneous total mass evaporation rate of the mixture can be then expressed as

$$\frac{dm_{mix}}{dt} = -\pi R D_w (\rho_w^{v,sat} - \rho_w^{v,\infty}) \frac{1}{\sqrt{1 + \cos(\theta)}}. \quad (7)$$

Environmental conditions, such as RH and T , play a crucial role in the evaporation behavior of the sessile droplet. The relative humidity is defined as the ratio of the actual partial pressure of water in the gaseous phase to the water vapor saturation pressure at the given T . The water vapor concentration at the interface between the droplet and the external gaseous phase is imposed to be determined by the water vapor saturation pressure of the droplet aqueous mixture at the given T . We assume an ideal gas behavior; therefore, the vapor water concentration at the interface can be expressed as

$$\rho_w^{v,sat} = \frac{P^{sol} M_w}{R_g T}, \quad (8)$$

where M_w and R_g are, respectively, the water molecular weight and the universal gas constant, while P^{sol} stands for the equilibrium vapor

pressure of the water solution forming the droplet. In fact, if a nonvolatile solute (e.g., salt and proteins, in the case of a saliva droplet) is contained within the drop, $\rho_w^{v,sat}$ depends on P^{sol} , which, in turn, is determined by the solute concentration that changes because of water evaporation (or condensation from the surrounding environment). In particular, P^{sol} can be expressed in the following way:

$$P^{sol} = (1 - x_s) \gamma_w P^{sat}, \quad (9)$$

where x_s is the salt (solute) molar fraction in the mixture, γ_w is the activity coefficient of water that depends on x_s , and P^{sat} is the equilibrium vapor pressure at the given T for pure water. The water vapor concentration in the bulk of the gaseous phase far from the droplet surface is assumed to be $\rho_w^{v,\infty} = RH \rho_w^{v,sat}$. The effect of droplet curvature on P^{sat} is neglected because, for a radius of curvature of 0.1 mm (within the range of 0.1–0.5 mm for a droplet volume of 10 nl and the observed initial contact angles), the increase in P^{sat} determined by the curvature of the surface is less than 0.1% as compared to that of a flat surface. There are two notable values of the water–vapor pressure at the droplet–air interface, P^{sol} , at $T = 25^\circ C$ (the ambient temperature considered in the first part of this study). These two values are 3153 and 2387 Pa, related, respectively, to the values of the initial c_{s0} and saturation c_s^{sat} salt concentration (with, respectively, x_{s0} and x_s^{sat} being the molar fractions). Obviously, these values change with ambient temperature.

B. Evaporation regimes

Three different regimes can be identified based on the assigned value of P^{sol} .^{17,18} In *regime I*, i.e., when the value of RH is greater than RH_0 (the threshold relative humidity that would be in equilibrium with the water activity, corresponding to the initial salt concentration),

$$RH \geq RH_0, \quad RH_0 = (1 - x_{s0}) \gamma_{w0}, \quad (10)$$

water condensates from the surrounding gaseous environment. Therefore, the droplet volume increases, diluting the solutes and, thus, promoting an increase also of the water activity [Fig. 1(a)]. In *regime II*, i.e., when RH is comprised between RH_0 and RH^{sat} (the threshold relative humidity that would be in equilibrium with the water activity, corresponding to the saturation salt concentration),

$$RH^{sat} \leq RH < RH_0, \quad RH_0 = (1 - x_{s0}) \gamma_{w0}$$

and

$$RH^{sat} = (1 - x_s^{sat}) \gamma_w^{sat}, \quad (11)$$

water evaporates from the liquid droplet. This evaporation promotes a gradual reduction of water activity within the drop due to the increase in salt concentration and the evaporation stops as soon as the water activity within the droplet matches the value that is in equilibrium with the selected value of RH [Fig. 1(b)]. In *regime III*, i.e., when the value of RH is smaller than RH^{sat} ,

$$RH < RH^{sat}, \quad RH^{sat} = (1 - x_s^{sat}) \gamma_w^{sat}, \quad (12)$$

it is again expected that water evaporates from the droplet, and that the volume decreases while the salt concentration increases with time until it reaches the precipitation concentration staying at this value until the water of the droplet completely evaporates [Fig. 1(c)].

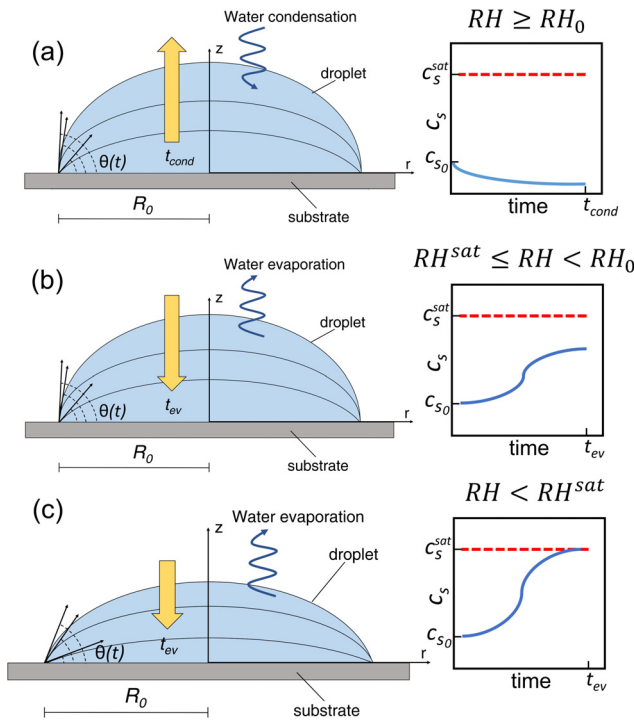


FIG. 1. Left panel of the figure details the scheme of a sessile droplet on a solid substrate undergoing condensation in (a) regime I and evaporation in (b) regime II and (c) regime III. Right panel reports the graphs detailing the behavior of the salt concentration c_s in the different regimes.

The RH^{sat} corresponds to the relative humidity at which the phenomenon of the *deliquescence* occurs, namely, the water-soluble salt (e.g., the sodium chloride) starts absorbing moisture from the surrounding air and forms a saturated aqueous solution.³² However, in most real cases, the aqueous salt solutions tend to precipitate not at the true saturation point, rather it forms supersaturated solutions. Indeed, salt precipitation occurs after the *efflorescence*, that is, nucleation and growth of salt crystals formed in the supersaturated state.³² In our case, since the choice of RH^{sat} value does not affect the qualitative conclusions, we illustrate the following modeling results with the assumption that the salt precipitation occurs at saturation point.

The instantaneous mass density rate can be expressed as follows:

$$\frac{d\rho_{mix}^l}{dt} = \frac{1}{V_{mix}} \frac{dm_{mix}}{dt} - \frac{\rho_{mix}^l}{V_{mix}} \frac{dV_{mix}}{dt}. \quad (13)$$

Data for aqueous solutions of sodium chloride were taken from Ref. 33 in the case of γ_s (salt activity coefficient) and γ_w [data from Ref. 33 have been fitted with the exponential relationship $\gamma_w = \exp(E_1 \cdot x_s^3/3 + E_2 \cdot x_s^2/2)$, where E_1 and E_2 are fitting parameters], and from Poling *et al.*³⁴ in the case of P^{sat} and ρ_{mix}^l (data from Ref. 34 have been fitted using the linear relationship $\rho_{mix}^l = C_1 \cdot x_s + C_2$, where C_1 and C_2 are fitting parameters) in the range of $x_{s0} < x_s < x_s^{sat}$ (salt molar fraction comprised between its initial value x_{s0} and the saturation value x_s^{sat}) and the investigated range temperatures (namely, 10–60 °C).

C. Wetting regimes

We confine our attention to the case in which we are in regime II or III, so that volume decrease in the droplet occurs by evaporation. The evaporation process of a sessile droplet on a flat surface is also influenced by the pinning behavior of the three-phase *contact line* (CL) that may or may not move toward different metastable positions, depending on the chemical and/or the structural heterogeneity of the solid substrate. Typically, in the condition of pinned CL, the droplet may undergo two dynamic CAs, namely, the *advancing contact angle* (θ_A , the maximum value of the CA at fixed wetting area) and the *receding contact angle* (θ_R , the minimum value of the CA at fixed wetting area).³⁵ These two values represent the limits in which the CA ranges at fixed wetting area, and their difference (namely, $\theta_A - \theta_R$) is widely known as *contact angle hysteresis* (CAH).

Generally, there may exist three typical wetting regimes, depending on the interaction between the sessile droplet and the substrate as well as the chemical–physical characteristics of the surface: the *constant contact radius* (CCR) condition, the *constant contact angle* (CCA) condition, and the *stick-slip* (SS) condition.^{30,31}

The CCR (fixed wetting area) is expected to occur in the case of hydrophilic surfaces, the initial contact between the substrate and the sessile droplet is characterized by a fast-spreading process during which the evaporation can be neglected, and the CR reaches its maximum value.³⁵ In the context of this work, the initial state of the droplet evaporation is imposed right after the spreading process that is assumed to occur instantaneously. Thus, we may assume $\theta_0 = \theta_{ep}$ imposing to the drop an initial configuration corresponding to the static equilibrium that would occur in the case of no evaporation. After the spreading, the droplet evaporates with a constant CR ($R = R_0$, $dR/dt = 0$), while its CA decreases from its initial value θ_0 to its final value θ_{final} (0 in the case of regime III) in a time span t_{CCR} , namely, the time elapsed for the droplet evaporation to attain the stationary state (i.e., a constant volume condition when we are in regime II, and a volume equal to zero when we are in regime III), see Fig. 2(a).³⁵ Therefore, for a sessile droplet evaporating in CCR mode, dV_{mix}/dt and dm_{mix}/dt [Eqs. (3) and (7), respectively] can be rewritten as follows:

$$\frac{dV_{mix}}{dt} = \frac{\pi R_0^3}{(1 + \cos \theta)^2} \frac{d\theta}{dt}, \quad R = R_0 \quad \text{and} \quad \frac{dR}{dt} = 0, \quad \theta_{final} < \theta < \theta_0, \quad (14)$$

$$\frac{dm_{mix}}{dt} = -\pi R_0 D_w (\rho_w^{v,sat} - \rho_w^{v,\infty}) f(\theta), \quad R = R_0, \quad \theta_{final} < \theta < \theta_0. \quad (15)$$

Equations (14) and (15) evidence that the two quantities are exclusively dependent on the CA, while the CR is a fixed parameter. By applying the total mass balance ($m_{mix} = m_s + m_w$, with m_s and m_w being the salt and water mass, respectively) and making explicit the mass density (ρ_{mix}^l), the water vapor concentration at the interface ($\rho_w^{v,sat}$) as well as the water activity (γ_w) in the instantaneous total mass evaporation rate (dm_{mix}/dt), Eqs. (13)–(15), can be rearranged to obtain the following set of equations:

$$\frac{dV_{mix}}{dt} = - \frac{M_w n_s}{(C_1 x_s + C_2) x_s^2} \frac{dx_s}{dt} - \frac{C_1 V_{mix}}{(C_1 x_s + C_2) x_s^2} \frac{dx_s}{dt}, \quad (16)$$

$$\frac{d\theta}{dt} = \frac{(1 + \cos \theta)^2}{\pi R_0^3} \frac{dV_{mix}}{dt}, \quad (17)$$

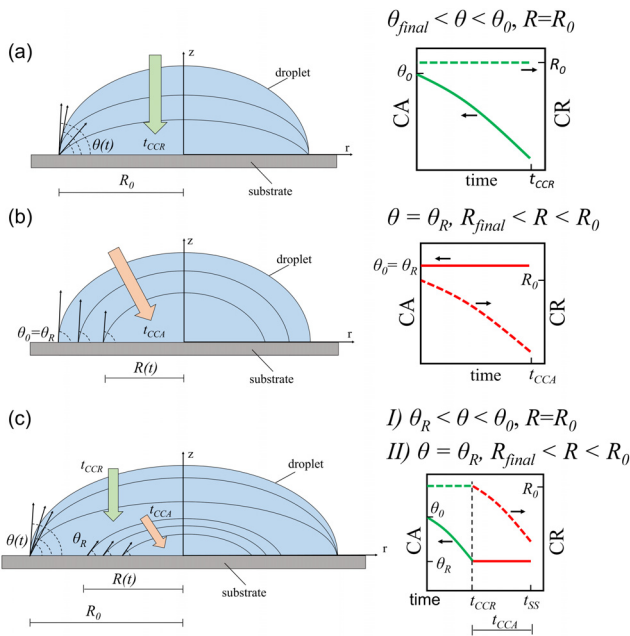


FIG. 2. Left panel of the figure details the scheme of a sessile droplet on a solid substrate undergoing evaporation in (a) CCR, (b) CCA, and (c) SS modes. Right panel reports the graphs detailing the behavior of the contact angle CA (solid line) and the contact radius CR (dashed line) in the different wetting regimes.

$$\frac{dx_s}{dt} = \frac{\pi R_0 D_w P^{sat}}{R_g T n_s} \frac{\left[\exp\left(E_1 \frac{x_s^3}{3} + E_2 \frac{x_s^2}{2}\right) (1 - x_s) - 1 \right]}{\sqrt{1 + \cos(\theta)}} x_s^2. \quad (18)$$

In this case, the unknowns to be determined are $V_{mix}(t)$, $\theta(t)$, and $x_s(t)$ that are all dependent on time (t). The set of Eqs. (16)–(18) provides a full description of the CCR stage. It is worth noticing that the differential equations are characterized by the presence of non-constant coefficients and also some unknown functions to be integrated, like $\theta(t)$ and $x_s(t)$ that appear nonlinearly; as a consequence, the system of (coupled) differential equations is not amenable to an analytical solution, and the set of equations describing each wetting stage is, thus, obtained numerically. When solved by numerical methods, this set of equations provides the results, which are shown in Sec. III.

When the sessile droplet is in contact with a hydrophobic surface with negligible CAH, the CCA is expected to be dominant due to the negligible CAH. Here, there is no spreading of the sessile droplet due to the intrinsic nature of the hydrophobic substrate; thus, we may directly assume $\theta_0 = \theta_{eq}$. In CCA mode, the droplet evaporates with a constant CA ($\theta = \theta_0 = \theta_R$, $d\theta/dt = 0$) while its CR decreases from its initial value R_0 to its final value R_{final} in a time span t_{CCA} , namely, the time elapsed for the droplet evaporation to attain the stationary state (i.e., a constant volume condition when we are in regime II), see Fig. 2(b).³⁵ Therefore, for a sessile droplet evaporating in CCA mode, Eqs. (3) and (7) can be rewritten as follows:

$$\frac{dV_{mix}}{dt} = 3\pi R^2 g(\theta_R) \frac{dR}{dt}, \quad \theta = \theta_0 = \theta_R \quad \text{and} \quad \frac{d\theta}{dt} = 0, \quad (19)$$

$$R_{final} < R < R_0,$$

$$\frac{dm_{mix}}{dt} = -\pi R D_w (\rho_w^{v,sat} - \rho_w^{v,\infty}) f(\theta_R) \theta = \theta_0 = \theta_R, \quad (20)$$

$$R_{final} < R < R_0.$$

In a similar way, Eqs. (19) and (20) indicate that these two quantities are dependent on the CR, while the CA remains a fixed parameter. Proceeding in the same manner as in the case of the CCR stage, Eqs. (13), (19), and (20) can be rearranged to have the following set of equations:

$$\frac{dV_{mix}}{dt} = -\frac{M_w n_s}{(C_1 x_s + C_2) x_s^2} \frac{dx_s}{dt} - \frac{C_1 V_{mix}}{(C_1 x_s + C_2) x_s^2} \frac{dx_s}{dt}, \quad (21)$$

$$\frac{dR}{dt} = \frac{1}{3\pi R^2 g(\theta_R)} \frac{dV_{mix}}{dt}, \quad (22)$$

$$\frac{dx_s}{dt} = \frac{\pi R D_w P^{sat}}{R_g T n_s} \frac{\left[\exp\left(E_1 \frac{x_s^3}{3} + E_2 \frac{x_s^2}{2}\right) (1 - x_s) - 1 \right]}{\sqrt{1 + \cos(\theta_R)}} x_s^2. \quad (23)$$

In this case, the unknowns to be determined are $V_{mix}(t)$, $R(t)$, and $x_s(t)$ that again are all dependent on time (t). The set of Eqs. (21)–(23) provides a full description of the CCA stage. When solved numerically, this set of equations provides the results, which are shown in Sec. III.

Finally, the SS condition is characterized by an initial CCR followed by CCA: at the beginning, the droplet undergoes the CCR condition for which the CA decreases from its initial value θ_0 to the intermediate value of θ_R , while the CR remains at its initial value R_0 . The equations that describe this first part of the SS regime can be rewritten as

$$\frac{dV_{mix}}{dt} = \frac{\pi R_0^3}{(1 + \cos \theta)^2} \frac{d\theta}{dt}, \quad R = R_0 \quad \text{and} \quad \frac{dR}{dt} = 0, \quad \theta_R < \theta < \theta_0, \quad (24)$$

$$\frac{dm_{mix}}{dt} = -\pi R_0 D_w (\rho_w^{v,sat} - \rho_w^{v,\infty}) f(\theta), \quad R = R_0, \quad \theta_R < \theta < \theta_0. \quad (25)$$

When the CA reaches the value of the receding CA, θ_R , the evaporating sessile droplet switches from the CCR to CCA condition, see Fig. 2(c). From that point onward, the CA keeps the value θ_R and remains constant, while the CR decreases from the initial value R_0 to R_{final} in the span t_{CCA} , namely, the time needed for droplet evaporation to attain the stationary state. The equations that describe the second part of the SS condition are

$$\frac{dV_{mix}}{dt} = 3\pi R^2 g(\theta_R) \frac{dR}{dt}, \quad \theta = \theta_R \quad \text{and} \quad \frac{d\theta}{dt} = 0, \quad R_{final} < R < R_0, \quad (26)$$

$$\frac{dm_{mix}}{dt} = -\pi R D_w (\rho_w^{v,sat} - \rho_w^{v,\infty}) f(\theta_R) \theta = \theta_R, \quad R_{final} < R < R_0. \quad (27)$$

Analogous to the case of both the single CCR and CCA stages, in the first part of the SS stage, $V_{mix}(t)$, $\theta(t)$, and $x_s(t)$ can be determined numerically by solving the set of Eqs. (16)–(18) with the conditions specified in Eqs. (24) and (25), while, in the second part, the variables become $V_{mix}(t)$, $R(t)$ [instead of $\theta(t)$], and $x_s(t)$, and they can be

determined numerically by solving the set of Eqs. (21)–(23) with the conditions specified in Eqs. (26) and (27).

The time span that ranges from 0 to $t_{SS} = t_{CCR} + t_{CCA}$ comprises the whole aforementioned process. The CCR and CCA regimes are generally considered as the extreme cases of the SS regime when $\theta_R = \theta_{final}$ in the first case and $\theta_R = \theta_0$ in the second case, with θ_R being the critical parameter that modulates the interconnection between these two regimes.³⁰

The SS mode represents the wetting behavior of more actual relevance, especially for hydrophobic surfaces, while the CCR is often observed to be the dominant regime in the case of hydrophilic surfaces.^{31,36,37} The evaporation process of a sessile droplet is characterized by a final mixed stage in which both the CA and the CR decrease until the droplet completely disappears. However, the elapsed time for this stage is much smaller than the time required for a complete evaporation of the sessile droplet and, thus, this stage can be neglected in comparison to the overall process.³⁸

III. RESULTS AND DISCUSSION

In this section, we first validate the proposed model against some experimental data reported by Souliè *et al.*,³⁹ which measured the volume decrease in NaCl–H₂O evaporating sessile droplets placed on thermal silicon wafers. Figure 3 reports the comparison between the experimental data and the theoretical curves provided by the model for the normalized volume profiles at different RHs [Fig. 3(a)] and θ_0 [Fig. 3(b)]. Modeling predictions are in good agreement with the experimental data (with an average relative deviation lower than 5% for each curve) and, in this case, an evaporation behavior of sessile droplets characterized by a CCR³⁹ is observed. This is quite remarkable since no fitting parameters were used.

To provide a convincing theoretical interpretation of the evaporation behavior of a sessile droplet under the different aforementioned regimes and conditions, two case studies are analyzed in the following. In the first case, the effect of the surface wettability, such as θ_0 and θ_R , is examined while, in the second case, the effect of environmental parameters such as RH and T is addressed.

A. Effect of the wetting regimes on the evaporation process

As a first case study, we report an analysis of the behavior of an evaporating sessile droplet aimed at providing an assessment of its

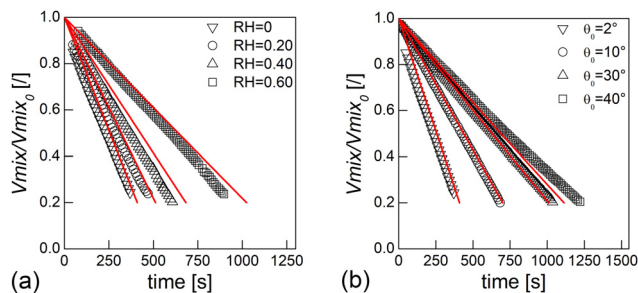


FIG. 3. V_{mix}/V_{mix0} as a function of time at (a) increasing RH and $\theta_0 = 2^\circ$ as well as at (b) increasing θ_0 and RH=0. Model parameters were $V_{mix0} = 10 \mu\text{l}$, $T = 25^\circ\text{C}$, $Dw = 2.52 \times 10^{-5} \text{ m}^2/\text{s}$, $P_0^{sat} = 3366 \text{ Pa}$, and $c_{s0} = 0.05844 \text{ kg/m}^3$. Red lines represent the theoretical curves provided by the model, and symbols represent the experimental results from Ref. 39.

dependence on the relevant geometrical parameters. This is useful to accurately design new surfaces with the purpose of modulating the evaporation time and, thus, possibly reduce the virus viability. To this aim, the cases of a droplet undergoing different wetting regimes have been considered. In the case of CCR, simulations were carried out at $T = 25^\circ\text{C}$ and $RH = 0.80$ (regime II) and for five different values of θ_0 (i.e., $30^\circ, 45^\circ, 60^\circ, 75^\circ, 90^\circ$) to simulate different hydrophilic substrate materials, for which the CCR behavior is the one that is typically observed.^{38,40} Then, in the case of CCA behavior, the environmental conditions considered are $T = 25^\circ\text{C}$, $RH = 0.80$ (regime II), and for five different values of θ_0 (i.e., $105^\circ, 120^\circ, 135^\circ, 150^\circ, 165^\circ$) to simulate surfaces with several degrees of hydrophobicity.⁴⁰

The initial value of droplet volume has been assumed to be $V_{mix0} = 10 \text{ nl}$, a typical value falling within the volume distribution of saliva droplets (1–10 nl) originating from a sneeze or a cough that could deposit on a surface.²¹ As it will be discussed in Sec. III C, we chose $c_{s0} = 10 \text{ kg/m}^3$ as initial value of salt concentration, that is, the same value used to prepare the bulk lysogeny broth in which the virus is suspended in the experiments performed by Lin and Marr.²⁰ The two values chosen for V_{mix0} and c_{s0} have been used both for the cases of the CCR and CCA behavior. Moreover, a relative humidity of 0.80 was chosen so that the analysis is conducted within regime II. In this way, it was possible to better clarify the droplet behavior when no water condensation from the surrounding atmosphere or salt precipitation within the droplet occurs (see Fig. 1).

Results obtained for the cases mentioned above are reported in Fig. 4 in terms of time evolution of the normalized CA ($\bar{\theta} = \theta/\theta_0$), CR ($\bar{R} = R/R_0$), mixture volume ($\bar{V} = V_{mix}/V_{mix0}$), and salt concentration ($\bar{c}_s = c_s/c_s^{sat}$). The upper part of the panel [Figs. 4(a)–4(c)] reports the results obtained in the case of CCR condition for a drop of aqueous solution deposited on a hydrophilic surface. It can be seen that $\bar{\theta}$ and \bar{V} decrease linearly until the end of the transient, which is in fact a behavior typically observed in the case of evaporation of sessile droplets on hydrophilic surfaces.⁴⁰ Increasing values of θ_0 correspond to a longer value of the time needed for the sessile droplet to attain the stationary state, t_{CCR} . The higher is θ_0 , the larger is the non-linearity of the transient behavior, which is a typical feature of hydrophobic surfaces.⁴⁰ A similar behavior is presented by the salt concentration at increasing values of θ_0 , which always reaches a final value smaller than the saturation concentration ($\bar{c}_s < 1$).

The lower part of the panel [Figs. 4(d)–4(f)] reports the results obtained in the case of CCA condition for a drop of aqueous solution deposited on a hydrophobic surface. In this case, the effect of θ_0 on the geometric evolution of the droplet is less significant, and all the curves display closer values. Notably, in contrast to the case of the CCR mode, a shorter time is needed for the sessile droplet to attain the stationary state, t_{CCA} , at increasing values of θ_0 . Figure 4(e) shows that the mixture volume follows a $-2/3$ power law as a function of time, which is typical for the CCA mode.⁴⁰ The following equation, which is typically utilized to describe the CCA mode of an evaporating sessile droplet,^{24,26,38} can be adopted to extrapolate the linear slope of a $\bar{V}^{2/3}$ vs time curve to evaluate the evolution of the CCA behavior at different θ_0 :

$$\bar{V}^{2/3} = \bar{V}_0^{2/3} + k \cdot t, \tag{28}$$

where $\bar{V}_0^{2/3}$ and k are, respectively, the initial value of the normalized mixture volume and the linear slope coefficient. The results of the

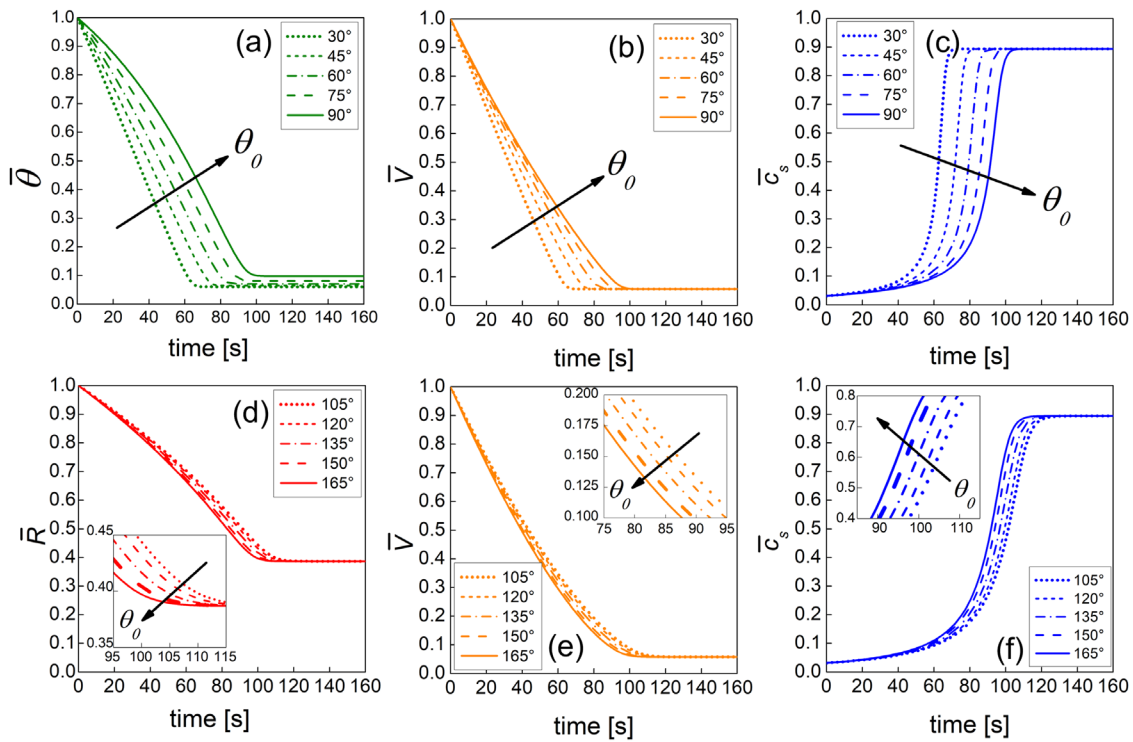


FIG. 4. Results of model simulations of the evaporation process of a sessile drop of aqueous solution with $V_{mix0} = 10$ nl and $c_{s0} = 10$ kg/m³ at a $RH = 0.80$ and $T = 25$ °C. The upper part of the panel details the CCR regime in terms of time evolution of the normalized (a) contact angle θ , (b) volume V , and (c) the salt concentration \bar{c}_s ; the lower part of the panel details the CCA regime in terms of time evolution of the normalized (d) contact radius \bar{R} , (e) volume V , and (f) the salt concentration \bar{c}_s . Results shown in (a)–(c) were obtained from Eqs. (16)–(18), while results shown in (d)–(f) were obtained from Eqs. (21)–(23).

fitting procedure (applied in the time interval 0–115 s) are reported in Table I, and R^2 coefficients indicate a good agreement with the observed behavior, while k decreases with θ_0 , thus, indicating a faster evaporation rate of the sessile droplet with the increasing initial CA in CCA mode. From Figs. 4(c) and 4(f), it is evident that \bar{c}_s always approaches the same final value, thus, indicating that change of θ_0 (for both the CCA and CCR modes and for the range of explored values) is a crucial factor in only determining the instant in which the stationary state is attained.

In the case of the SS condition, simulations were carried out at $T = 25$ °C, $RH = 0.80$, $\theta_0 = 60^\circ$, and for several values of θ_R (i.e., 30°,

35°, 40°, 45°, 50°, and 55°) to appreciate the effect of the receding CA on the evaporation process. Also, for this case study, the assumed initial values for the droplet volume was $V_{mix0} = 10$ nl and for salt concentration, $c_{s0} = 10$ kg/m³. The initial stage of the evaporation process is dominated by the CCR mode; therefore, the droplet evaporates with a fixed CL ($R = R_0$), while the CA decreases from θ_0 to θ_R .

Figure 5(a) depicts the initial decrease in the CA down to the value of θ_R (violet-colored round marker), while the CR maintains its initial value R_0 [Fig. 5(b)]. Then, after the initial CCR stage, the evaporation proceeds according to a CCA regime, keeping a constant value of the CA equal to θ_R while the CR starts decreasing to approach a

TABLE I. Results of the fitting procedure applied by Eq. (28).

CCA stage			SS stage			
θ_0 (°)	k (s ⁻¹)	R^2	θ_0 (°)	θ_R (°)	k (s ⁻¹)	R^2
105	$-7.58 \times 10^{-3} (\pm 1 \times 10^{-5})$	0.999	60	30	$-8.72 \times 10^{-3} (\pm 2 \times 10^{-5})$	0.997
120	$-7.71 \times 10^{-3} (\pm 2 \times 10^{-5})$	0.999	60	35	$-8.52 \times 10^{-3} (\pm 2 \times 10^{-5})$	0.998
135	$-7.89 \times 10^{-3} (\pm 2 \times 10^{-5})$	0.999	60	40	$-8.35 \times 10^{-3} (\pm 2 \times 10^{-5})$	0.998
150	$-8.08 \times 10^{-3} (\pm 2 \times 10^{-5})$	0.999	60	45	$-8.19 \times 10^{-3} (\pm 2 \times 10^{-5})$	0.998
165	$-8.19 \times 10^{-3} (\pm 2 \times 10^{-5})$	0.999	60	50	$-8.05 \times 10^{-3} (\pm 2 \times 10^{-5})$	0.999
			60	55	$-7.90 \times 10^{-3} (\pm 2 \times 10^{-5})$	0.999

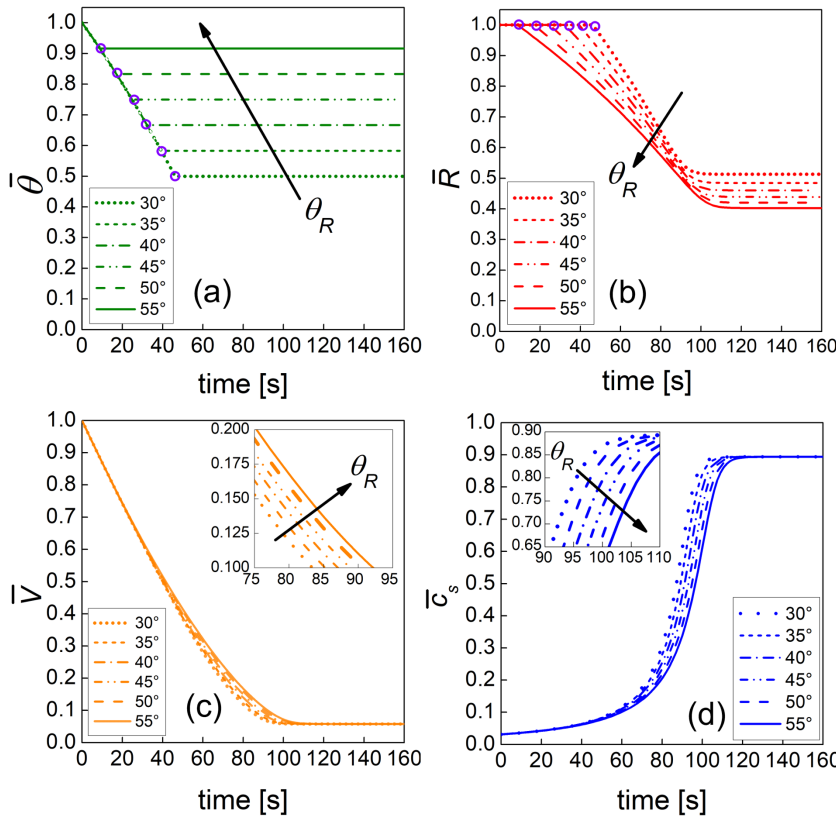


FIG. 5. Results of model simulations of the evaporation process of a sessile drop of aqueous solution undergoing SS with $V_{mix0} = 10$ nl, $c_{s0} = 10$ kg/m³, and $\theta_0 = 60^\circ$, at a $RH = 0.80$ and $T = 25^\circ\text{C}$, in terms of time evolution of the normalized (a) contact angle $\bar{\theta}$, (b) contact radius \bar{R} , (c) volume \bar{V} , and (d) the salt concentration \bar{c}_s . Round markers in the upper two figures indicate the instant in which the process undergoes from CCR to CCA in correspondence of θ_R . Results shown for the first part of the SS stage were obtained from Eqs. (16)–(18), while results shown for the second part of the SS stage were obtained from Eqs. (21)–(23).

stationary state. We may notice a non-linear behavior for the volume that roughly follows a $-2/3$ power law, similar to the case discussed before where evaporation follows a single CCA mode. Of course, the lower is the θ_R , the longer is the time needed for the start of the CCA condition. Also, in this case, the same fitting procedure by Eq. (28) was applied to calculations performed for the SS stage. As shown in Table I, the accuracy of Eq. (28) in describing experimental data increases (i.e., R^2 increases) as θ_R tends to θ_0 . Moreover, the fact that k increases with θ_R indicates a reduction of the evaporation rate of the sessile droplet as θ_R increases as well.

Indeed, Figs. 5(a) and 5(b) show that the t_{CCR} inversely increases with θ_R , and, for each curve, a greater value of the final CA corresponds to a lower value of the CR. Moreover, it can also be observed that t_{CCA} increases with θ_R , and this stage seems to affect the transient more than the CCR stage. In fact, while \bar{V} and \bar{c}_s always approach the same final value [Figs. 5(c) and 5(d)], an increasing value of θ_R apparently induces a longer transient time span for both the mixture volume and the salt concentration.

Figure 6 reports a sort of abacus that summarizes the results in terms of the evaporation times as a function of θ_0 for a sessile droplet undergoing the three different evaporation modes: (a) t_{CCA} , in the case of a single CCA condition, (b) t_{CCR} , in the case of a single CCR condition, and (c) t_{SS} , in the case of the combined SS condition. The times related to the CCR curve are calculated when $\theta_R = 0^\circ$ and at different values of θ_0 , while those related to the CCA curve are calculated when $\theta_R = \theta_0$ and at different values of θ_0 and, finally, those related to the SS curve are calculated at a fixed value

of θ_R and for different values of θ_0 . In this latter case, several values of θ_R ($5^\circ, 10^\circ, 20^\circ, 30^\circ, 40^\circ, 50^\circ, 60^\circ$, and 70°) have been considered to determine the evaporation time on different wetting regimes. The other parameters used in the simulations were $T = 25^\circ\text{C}$, $RH = 0.80$, $V_{mix0} = 10$ nl, and $c_{s0} = 10$ kg/m³.

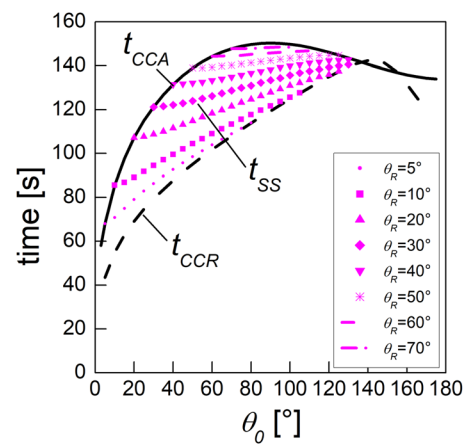


FIG. 6. Evaporation time as a function of θ_0 when the sessile droplet undergoes the CCA regime, t_{CCA} , the CCR regime, t_{CCR} , and the SS regime, t_{SS} . Parameters used in the simulations were $T = 25^\circ\text{C}$, $RH = 0.80$, $V_{mix0} = 10$ nl, and $c_{s0} = 10$ kg/m³.

If one hypothetically includes also the hydrophilic surfaces into the range of substrates on which it is possible to observe the CCA regime ($\theta_0 < 90^\circ$), from the graph it is possible to notice that t_{CCA} first increases with θ_0 and starts to slightly decrease beyond a threshold value located at around 90° . This observation suggests that, while for hydrophobic surfaces, the t_{CCA} does not display a significant dependence on θ_0 , the hydrophilic surface may be treated to modulate the initial CA so that t_{CCA} would be minimized. In the same way, if one includes the hydrophobic surfaces ($\theta_0 > 90^\circ$) in the substrates applicable to the CCR regime, it can be observed that t_{CCR} increases for almost the entire range of θ_0 until a threshold value of about 150° . This occurrence evidences that both the hydrophilic and the hydrophobic substrates may be re-designed to increase the droplet wettability and consequently reduce the evaporation time. The graph suggests that, for CAs greater than the observed threshold value (around 140°), t_{CCR} would decrease if the droplet hydrophobicity is enhanced. However, this observation may appear inconsistent as the wetting behavior on the superhydrophobic surfaces ($\theta_0 > 150^\circ$) is still not well-clarified.⁴⁰ Interestingly, curves of t_{SS} appear to be comprised between t_{CCA} and t_{CCR} , giving more emphasis to the observation that the pure CCA and the pure CCR regimes are the extreme cases of the SS regime when $\theta_R = \theta_0$ and $\theta_R = 0^\circ$, respectively.⁴⁰ The plot in Fig. 6 shows that t_{SS} increases with θ_0 , according to the trends already observed for t_{CCA} and t_{CCR} . Moreover, t_{SS} increases at higher θ_R , revealing that the droplet undergoes primarily the CCA regime when the receding CA gets progressively closer to the initial CA and

confirming that the θ_R plays a crucial role in the lifetime of the sessile droplet. This behavior may further suggest that materials with very high θ_R could lead to longer evaporation times. Therefore, several surfaces may be designed on purpose to decrease the θ_R and, thus, reduce t_{SS} .

B. Effect of the environmental conditions on the evaporation process

As a second case of study, a systematic analysis has been conducted on the different environmental regimes (namely, regime II and III) to evaluate the different physical phenomena that may take place during the evaporation. In fact, a selected combination of T and RH may lead to a significant difference in the timescales related to the evaporation rate of the droplet (from a few hours to many days³¹) and may determine if salt precipitation, which affects the virus viability, does or does not occur. The results of this analysis are summarized in Figs. 7 and 8 in terms of time evolution of the normalized CA ($\bar{\theta} = \theta/\theta_0$), CR ($\bar{R} = R/R_0$), mixture volume ($\bar{V} = V_{mix}/V_{mix0}$), and salt concentration ($\bar{c}_s = c_s/c_s^{sat}$) at different RH s and T . Here, simulations were carried out by adopting a SS mode as it represents a case of actual relevance.

For the assessment of the RH effect, the values chosen for the parameters were $T = 25^\circ\text{C}$, $\theta_0 = 120^\circ$, $\theta_R = 80^\circ$, and four different values of RH (i.e., 0.20, 0.40, 0.60, 0.80) to simulate the different evaporation behaviors in the conditions dictated by regime II and III. Hence, we consider here only conditions for which $RH < RH_0$,

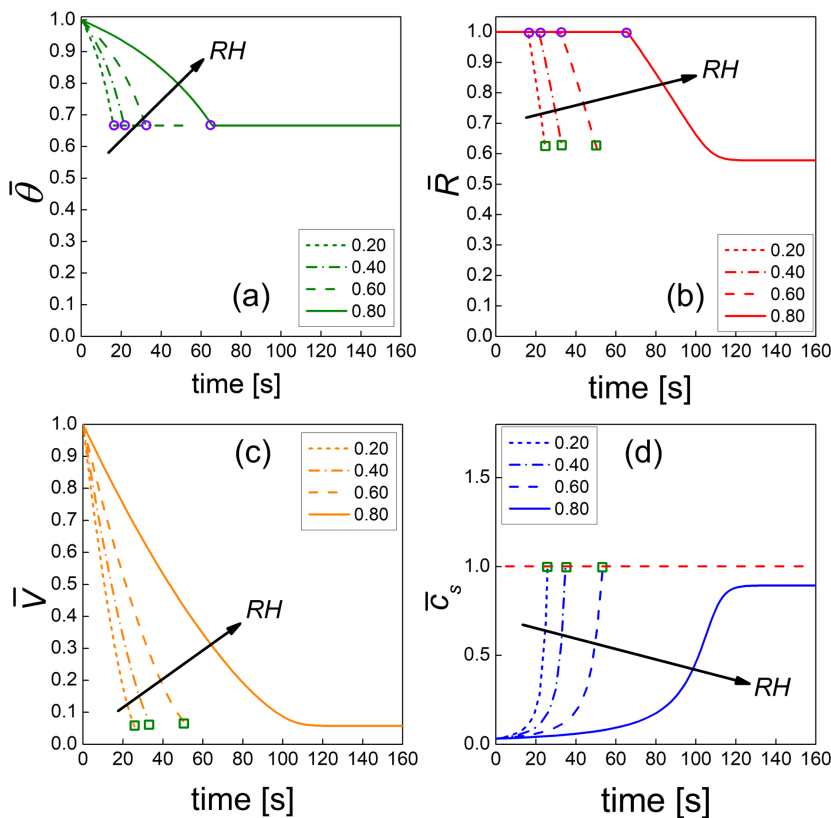


FIG. 7. Results of model simulations of the evaporation process of a sessile drop of aqueous solution submitted to different RH conditions with $V_{mix0} = 10$ nl, $c_{s0} = 10$ kg/m³, $T = 25^\circ\text{C}$, and at $\theta_0 = 120^\circ$ and $\theta_R = 80^\circ$, in terms of time evolution of the normalized (a) contact angle $\bar{\theta}$, (b) contact radius \bar{R} , (c) volume \bar{V} , and (d) the salt concentration \bar{c}_s . Round markers in the upper two figures indicate the instant in which the process undergoes from CCR to CCA in correspondence to θ_R , while square markers in (b)–(d) indicate the instant in which the related profiles are truncated. Results shown for the first part of the SS stage were obtained from Eqs. (16)–(18), while results shown for the second part of the SS stage were obtained from Eqs. (21)–(23).

Downloaded from http://pubs.aip.org/aip/phf/article-pdf/doi/10.1063/5.0143813/1736933/057109_1_5.0143813.pdf

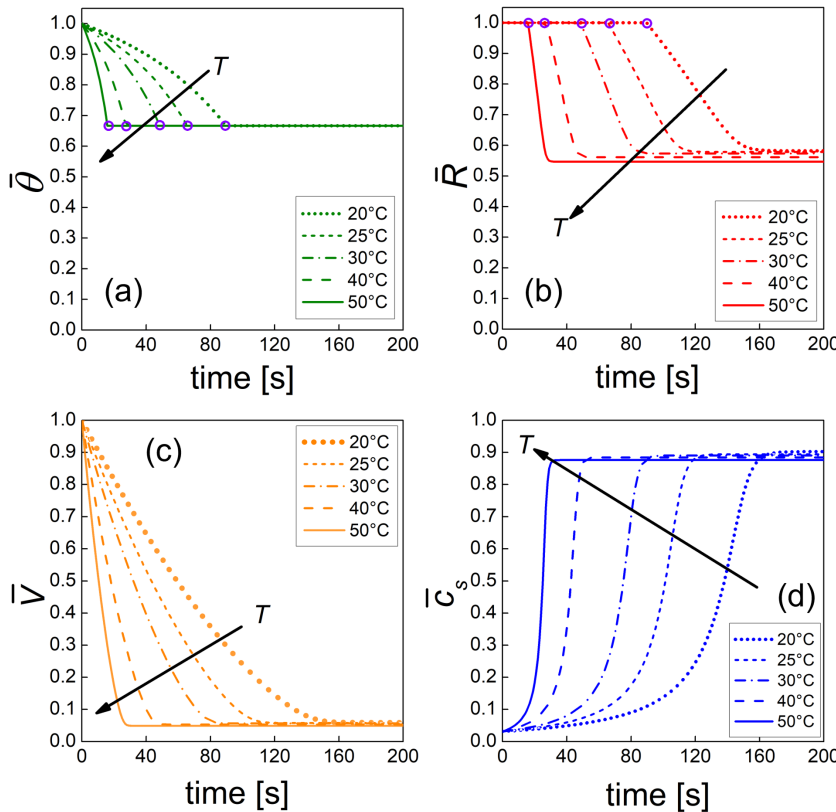


FIG. 8. Results of model simulations of the evaporation process of a sessile drop of aqueous solution at different values of T with $V_{mix0} = 10$ nl, $c_{s0} = 10$ kg/m³, $RH = 0.80$, and at $\theta_0 = 120^\circ$ and $\theta_R = 80^\circ$, in terms of time evolution of the normalized (a) contact angle $\bar{\theta}$, (b) contact radius \bar{R} , (c) volume \bar{V} , and (d) the salt concentration \bar{c}_s . Round markers in the upper two figures indicate the instant in which the process undergoes from CCR to CCA in correspondence to θ_R . Results shown for the first part of the SS stage were obtained from Eqs. (16)–(18), while results shown for the second part of the SS stage were obtained from Eqs. (21)–(23).

i.e., when the volume of the drop decreases by evaporation. For the assessment of the effect of T , the values chosen for parameters were $RH = 0.80$, $\theta_0 = 120^\circ$, $\theta_R = 80^\circ$, and five different values of T (i.e., 20, 25, 30, 40, and 50 °C). For both cases, the initial values for the droplet volume was again assumed to be $V_{mix0} = 10$ nl and for the salt concentration, $c_{s0} = 10$ kg/m³.

As the relative humidity of the surrounding environment increases, the driving force for evaporation of the sessile droplet decreases. For this reason, longer evaporation times are observed at greater values of RH . Figures 7(a) and 7(b), show that an increase in RH leads to longer t_{CCR} , corresponding to a longer time elapsed for the CA to attain the value of θ_R and, consequently, to a delayed CCA stage. Moreover, an increase in t_{CCA} is also observed; thus, an increase in the whole time of the process is expected [Fig. 7(c)]. The volume profile is described by a non-linear behavior that becomes more prominent as RH values increase and follows a decreasing $-2/3$ power law, as already observed in the first case study [see Figs. 4(e) and 5(c)]. The most prominent effect of the relative humidity is reported in Fig. 7(d), which shows that, for values of RH increasing from 0.2 to 0.6, the salt concentration would exceed the saturation value and, thus, lead to salt crystallization and precipitation (regime III, $RH < RH^{sat}$), while, in the case of $RH = 0.80$, no salt precipitation occurs (regime II, $RH^{sat} \leq RH < RH_0$) as the concentration remains under the threshold value. Therefore, as stated in Sec. II, we assumed that salt precipitation physically occurs at the saturation value (neglecting the supersaturation state), and we consistently truncated all the profiles when the salt

concentration profile attained the saturation value at the red dashed line ($\bar{c}_s = 1$). Square markers indicate the instant in which the salt concentration takes the saturation value.

Conversely, as T increases, shorter values of t_{CCR} are predicted, corresponding to a reduced time needed for the CA to attain the value of θ_R and, consequently, to an anticipated CCA stage and to a decrease in t_{CCA} as well [see Figs. 8(a) and 8(b)]. We recall the expression given in Eq. (7) for the instantaneous total mass evaporation rate (dm_{mix}/dt) to better elucidate the effect of environmental temperature on the evaporation rate. This quantity is dependent on both the water diffusion coefficient (D_w) and the water vapor concentration ($\rho_w^{v,sat}$) that, in turn, is dependent on the saturation pressure. As the saturation pressure is related to the amount of water vapor held in the air at a specific T , at higher temperatures, air can hold more water vapor considering even the exponential relationship between T and P^{sat} .³⁴ This difference contributes to a faster evaporation rate of the sessile droplet. As D_w also increases with T ,^{21,22} a further contribution to a faster evaporation process is also expected.

Also in this case, the volume profile is described by a non-linear behavior that becomes less evident at increasing T and follows a decreasing $-2/3$ power law [see Fig. 8(c)]. The effect of temperature on the salt concentration is manifested in a shorter transient interval and the final value is always attained below the saturation threshold as $RH = 0.8$. In cases of $RH < RH^{sat}$, higher temperatures would decrease the transient interval to arrive at $\bar{c}_s = 1$. Therefore, as explained in the description of the three regimes, the temperature does not determine

whether crystallization occurs or not but it influences the transient interval.

Figure 9 reports the evaporation times of the sessile droplet under regime II (curves included between the two limits of RH_0 and RH^{sat}) and in the SS condition, as a function of RH . Several values of T (10, 20, 25, 30, 40, 50, and 60 °C) have been considered to determine the evaporation times in different environmental conditions. Other parameters used in the simulations were $\theta_0 = 120^\circ$, $\theta_R = 80^\circ$, $V_{mix0} = 10$ nl, and $c_{s0} = 10$ kg/m³. The graph shows that t_{SS} monotonically increases with the RH due to the decreasing driving force for evaporation. Notably, the t_{SS} is always monotonically increasing with RH and decreases with T . The higher the temperature, and the lower the relative humidity, the shorter is the evaporation time to reach $\bar{c}_s = 1$.

C. Relative viability (RV) of the virus

The illustrated behavior has obvious consequences on the viability of the virus suspended within a droplet, as will be assessed in the following. The virus present within the droplet is exposed to several solute components of the mixture (e.g., salt), with a harmful cumulative exposure that affects its viability. The longer the time of exposure and the higher the solutes concentration, which are parameters whose values are ruled by the drop evolution during exposure to the environmental conditions, the lower is the virus viability. In fact, several studies have pointed out^{18–20} that a solute concentration different from the physiological value (difference induced by the water evaporation or condensation) establishes an osmotic gradient between the inside and outside of enveloped viruses. Therefore, the virus may shrink or swell, depending on the solution being hypertonic or hypotonic,⁴¹ and combined with several conditions such as temperature, pH, and exposure time, may irreversibly damage the virus structure. Cordova *et al.*⁴² pointed out that after certain exposure time (~ 15 min for T-phage virus), the high salt concentration is established inside the capsid and that “during the rapid dilution [contact with the mucosae or experimental dilutions] there is not enough time for the salt ions to leave the capsid; rather, only more water diffuses in, resulting in an osmotic

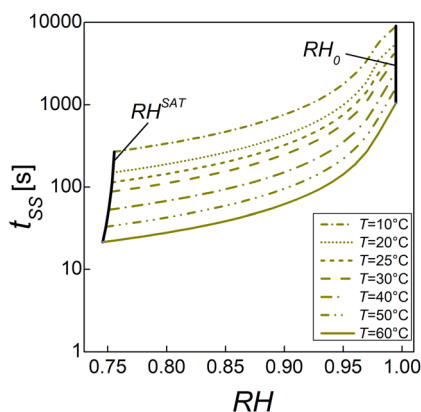


FIG. 9. Evaporation times (reported on a logarithmic scale of base 10) as a function of RH when the sessile droplet undergoes regime II and the SS mode. Parameters used in the simulations were $\theta_0 = 120^\circ$ and $\theta_R = 80^\circ$, $V_{mix0} = 10$ nl and $c_{s0} = 10$ kg/m³.

pressure that ruptures the capsid at a critical value of the incubation salt concentration.” As suggested by the previous discussion, by numerically solving the set of equations analyzed in Sec. II, several parameters of interest can be computed, such as the CA, the CR, the mixture volume, and the salt concentration, which play a relevant role in determining the virus viability. With the aim of estimating virus viability, one should first introduce a quantitative indicator of the effect of virus exposure to harmful factors. We introduce a quantity that lumps together the effects of all the relevant factors and accounts for exposure time and conditions. This is the so-called *cumulative dose* (CD) that represents the integral over time of the salt concentration and is used to measure the damage accumulation to the structure of the virus,²⁰

$$CD = \int_0^\tau c_s(t) dt, \quad (29)$$

where c_s [kg m⁻³] is the salt concentration, which can be calculated from our previous model simulations, while τ stands for the time at which one evaluates CD [kg s m⁻³]. When CD attains a *critical* value, one can assume the virus to be inactivated. The criterion to select this *critical* value depends on the virus and represents a threshold above which the probability of virus survival is below a selected value. As already reported in our previous work,²⁵ we referred to the experiments performed by Lin and Marr²⁰ to determine a reasonable viability of the virus as a function of the CD . In their work, these authors experimentally studied the viability of the virus MS2, a model for non-enveloped viruses that is widely used in environmental engineering studies, incubated in a bulk lysogeny broth at different ionic strengths at 22 °C. They reported the *relative viability* (RV) of MS2, defined as the ratio of the MS2 post-exposure concentration to its pre-exposure concentration, as a function of the CD of sodium chloride. Using a power law function to fit these experimental data, we obtained the following expression describing the dependence of RV on CD :²⁵

$$RV = 1 - 0.0095 (CD)^{0.24}, \quad (30)$$

where 0.0095 and 0.24 are parameters obtained to best fit the experimental data. Under the assumption that such a relationship holds true also at a temperature below and above 22 °C, we combined Eq. (30) with the calculations performed with the proposed model for droplet evaporation, to estimate the RV of a virus as a function of the CD , at prescribed conditions of RH and T , for selected substrate materials (i.e., at assigned θ_0 and observed θ_R), and for a given initial volume and salt concentration of the droplet. Based on these considerations, we evaluated the CD and, in turn, RV for different substrate features (Fig. 10) and environmental conditions (Fig. 11). Once the RV plot is predicted, one can then exploit this information to estimate the survival time of the virus based on the threshold RV that has been selected. Therefore, we neglect the possible dependence of Eq. (30) on T and investigate the pure effect of T on the evaporative process, which has as a secondary effect at different dynamics of c_s . The specific physicochemical mechanism of inactivation of various viruses in evaporating droplets is not yet fully understood,⁴³ but in future works, with the implementation in the present evaporative model of other relations, which explicitly link the solution variables (c_s and T) and the time of exposure to RV of specific viruses, it will be possible to discern the contribution of the different factors in the general dynamics.

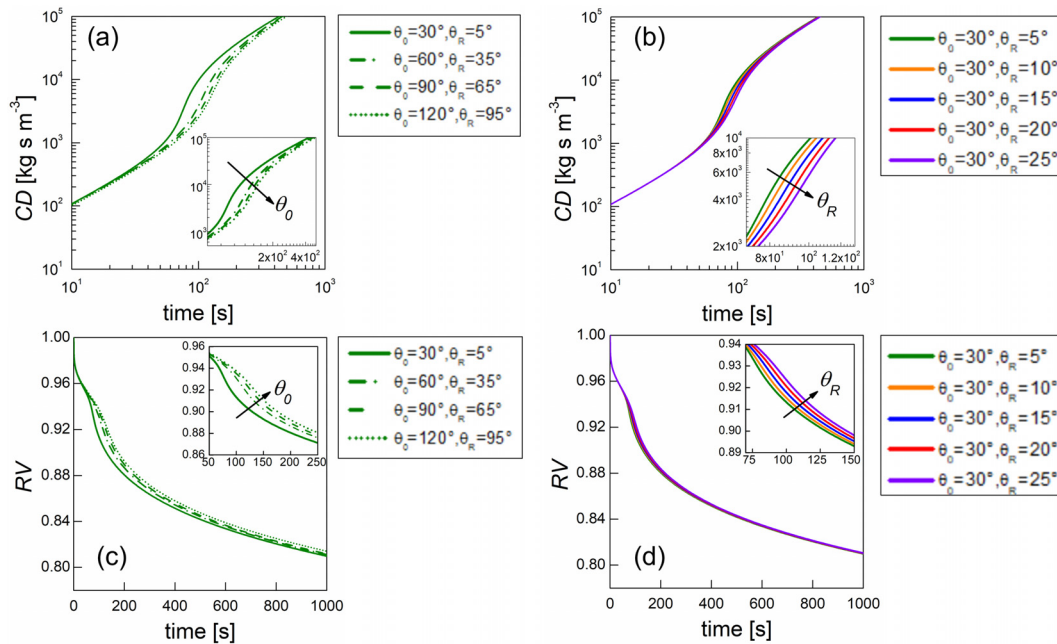


FIG. 10. Results of model simulations of the evaporation process of a sessile drop of aqueous solution in terms of cumulative dose (a) and (b), CD , and relative viability (c) and (d), RV . (a) and (c) Report the different tested θ_0 with $\Delta\theta = 25^\circ$. (b) and (d) Report the different tested θ_R with $\theta_0 = 30^\circ$. Other model parameters were $V_{mix0} = 10$ nl, $c_{s0} = 10$ kg/m³, $RH = 0.80$, and $T = 22^\circ\text{C}$. Results shown for the first part of the SS stage were obtained from Eqs. (16)–(18), while results shown for the second part of the SS stage were obtained from Eqs. (21)–(23), while Eqs. (29) and (30) were used for the whole SS stage.

For example, for an explicit dependence on T , assuming that a conformational change of a viral protein renders the virus inert, the rate of inactivation I has been described by the Arrhenius equation, $I_{max} e^{-\frac{E_a}{k_B T}}$, where I_{max} is the maximum inactivation rate at high temperature, E_a an activation energy, and k_B the Boltzmann constant.^{44,45}

1. Effect of the wetting regimes on the virus viability

Figure 10 reports the time evolution of the cumulative dose and the relative viability at different θ_0 (i.e., 30° , 60° , 90° , and 120°) with a fixed $\Delta\theta$ ($\theta_0 - \theta_R$) of 25° [Figs. 10(a) and 10(c)], and different θ_R (i.e., 5° , 10° , 15° , 20° , and 25°) with a fixed $\theta_0 = 30^\circ$ [Figs. 10(b) and 10(d)]. Model parameters were $V_{mix0} = 10$ nl, $c_{s0} = 10$ kg/m³, $RH = 0.80$, and $T = 22^\circ\text{C}$ so that the virus viability can be assessed in the case of regime II with no salt precipitation occurring. In this case, it can be observed that an increase in the CD is accompanied by a decrease in the RV and a sensible effect of the CA is present in the early stages of the process.

Insets in Figs. 10(a) and 10(c) indicate, in the selected time window and adopted conditions, a slight dependence of CD and RV on θ_0 , showing that these two parameters slow down with the increasing initial CA of the surface on which the droplet is deposited. This result is in line with the recent experimental evidence that virus contained in sessile droplets tends to survive more on commercial polymers than on glass (usually characterized by lower CA s).⁴⁶ Nevertheless, we underline that the proposed model, under the assumptions discussed in Sec. II, with the adopted conditions and the approach selected to assess the virus viability, does not capture the experimental evidence of

a larger difference that may occur in the virus viability when the sessile droplet is placed on different surfaces. For instance, in Ref. 47, the authors measured the stability of SARS-CoV-2 in virus transport medium (measured in log unit of 50% tissue culture infectious dose [TCID50] per ml) and pipetted a $5\ \mu\text{l}$ droplet of virus culture on the selected surface at a room temperature of 22°C with a relative humidity of around 65%. It could be observed that the virus concentration of a droplet placed on a plastic material was almost two times greater than that of a droplet placed on glass after 2 days of incubation. In addition, insets in Figs. 10(b) and 10(d) also indicate that CD and RV , in a selected time window, tend to have a negligible dependence on the receding CA .

Indeed, it is then inferred from these results that on hydrophilic surfaces the virus viability is reduced, as the CCR mode, or SS mode approaching toward the CCR, is often observed for those types of surfaces. This observation is also in agreement with the behavior of the evaporation times observed in Fig. 6. Under this perspective, data reported in Figs. 6 and 10 may be consulted as a combined map of the evaporation times matching the requested RV values, at the exploited substrate features and wetting regimes, for giving useful indications to design new surfaces with the aim of reducing the virus viability. We underline that the effect of a solid surface on the viability of viruses placed inside a sessile droplet standing on it is not just limited to the wetting behavior of the droplet itself but should also include the effect of the chemical nature of the solid substrate, not accounted for in the current version of the model that is then suited only for the case of inactive substrates.

Downloaded from http://pubs.aip.org/aip/phf/article-pdf/doi/10.1063/5.0143813/1738933/057109_1_5.0143813.pdf

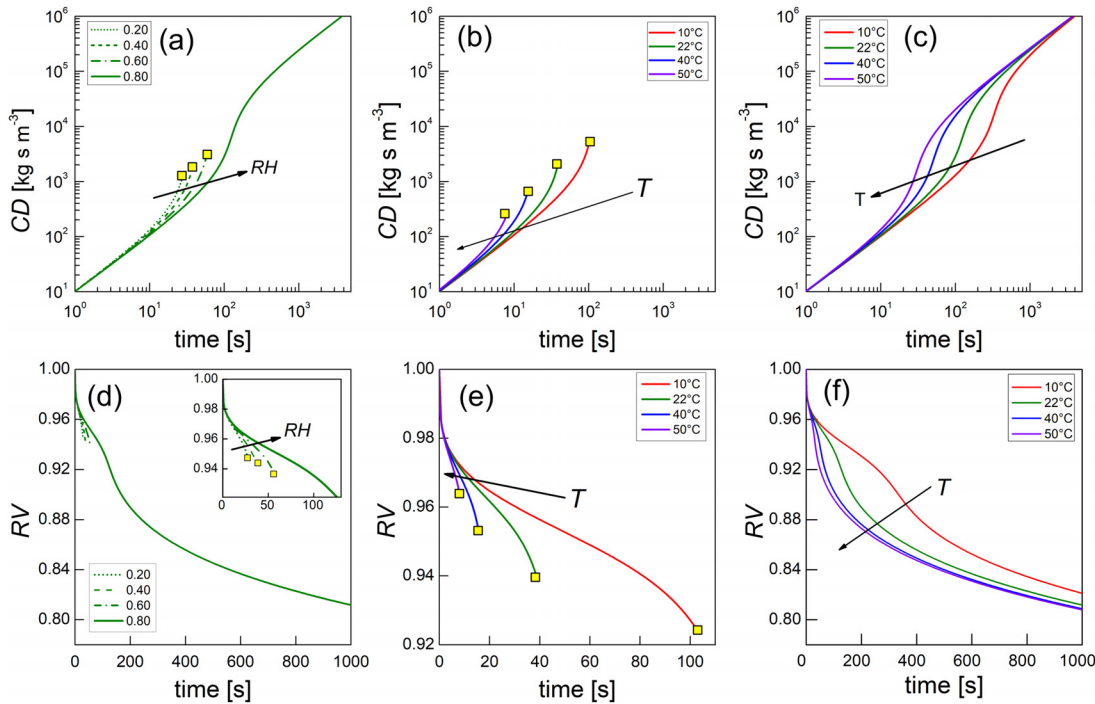


FIG. 11. Results of model simulations of the evaporation process of a sessile drop of aqueous solution in terms of cumulative dose (a)–(c), CD , and relative viability (d)–(f), RV . (a) and (d) Report the different tested RH at $T = 22^\circ\text{C}$. (b) and (e) Report the different tested T at $RH = 0.40$. (c) and (f) Report the different tested T at $RH = 0.80$. Other model parameters were $V_{mix0} = 10\text{ nl}$, $c_{s0} = 10\text{ kg/m}^3$, $\theta_0 = 120^\circ$, and $\theta_R = 80^\circ$. Square markers indicate the instant at which the salt concentration attains the saturation value. Results shown for the first part of the SS stage were obtained from Eqs. (16)–(18), while results shown for the second part of the SS stage were obtained from Eqs. (21)–(23), while Eqs. (29) and (30) were used for the whole SS stage.

2. Effect of the environmental conditions on the virus viability

Figure 11 reports the time evolution of the cumulative dose and the relative viability at three different cases: different RH (i.e., 0.20, 0.40, 0.60, and 0.80) at $T = 22^\circ\text{C}$ [Figs. 11(a) and 11(d)], and different values of T (i.e., 10, 22, 40, and 50°C), at $RH = 0.40$ [Figs. 11(b) and 11(e)] and $RH = 0.80$ [Figs. 11(c) and 11(f)]. Model parameters for this second case of study were $V_{mix0} = 10\text{ nl}$, $c_{s0} = 10\text{ kg/m}^3$, $\theta_0 = 120^\circ$, and $\theta_R = 80^\circ$ so that the virus viability can be assessed when the droplet evaporation undergoes the SS regime with and without salt precipitation. In this case, the environmental conditions appear to strongly influence the CD and, in turn, the RV . As expected, an increase in the relative humidity leads to longer times needed to reach a certain value of CD [Fig. 11(a)] and it always approaches different final values, while the RV dependence on the RH can be observed in the inset reported in Fig. 11(d). The effect of temperature on the CD and RV can be better appreciated in the other two cases, reporting that an increase in T leads to shorter times elapsed for the CD and RV to attain the same final values. In addition, Figs. 11(a) and 11(d) show that at RH of 0.20, 0.40, and 0.60, CD and RV curves are truncated (in correspondence of $c_s = c_s^{sat}$). In fact, we recall that, with a RH falling in regime III, the droplet completely evaporates before the CD required for inactivation may be attained, and the virus survives as it is no longer surrounded by a highly concentrated solution. In this way, the rapid drying reduces the exposure time to osmotic stresses⁴¹

and avoids achieving high salt concentration inside the capsid, which would cause an osmotic shock. In the same way, the effect of temperature can be appreciated even on the occurring salt saturation and precipitation. In fact, in the case of $RH = 0.40$ [Figs. 11(b) and 11(e)] and, therefore, regime III, it can be observed that CD and RV evolve faster at increasing T , and curves are truncated at $c_s = c_s^{sat}$ at progressively decreasing times. Conversely, in the case of regime II at $RH = 0.80$, the droplet settles in a condition of equilibrium with the surrounding air without attaining the saturation concentration. Therefore, the virus is subjected to high salt concentrations for a sufficient time leading to lower RV and then a higher mortality. This observation is mirrored by the experimentally determined U-shaped dependence on RH of the relative viability exhibited by other virus models reported in Refs. 17 and 19.

Also in this case, it would be useful to combine the information gathered from Fig. 7 with that from Fig. 11 to find the conditions that maximize the virus mortality and, therefore, reduce the infection spreading.

An overall picture of the effect of RH and T on RV of the MS2 virus at several evaporation times, as predicted by the proposed model, is reported in Fig. 12, where four temperature values have been considered (i.e., 10, 20, 22, and 40°C). Model parameters were $V_{mix0} = 1\ \mu\text{l}$, $c_{s0} = 10\text{ kg/m}^3$, and $\theta_0 = 86^\circ$ (initial CA for a polystyrene substrate⁴⁸). The notable results of the simulations are (i) the U-shaped dependence of RV on RH with a minimum value located within the regime II region (the same behavior occurs at each of the investigated values of

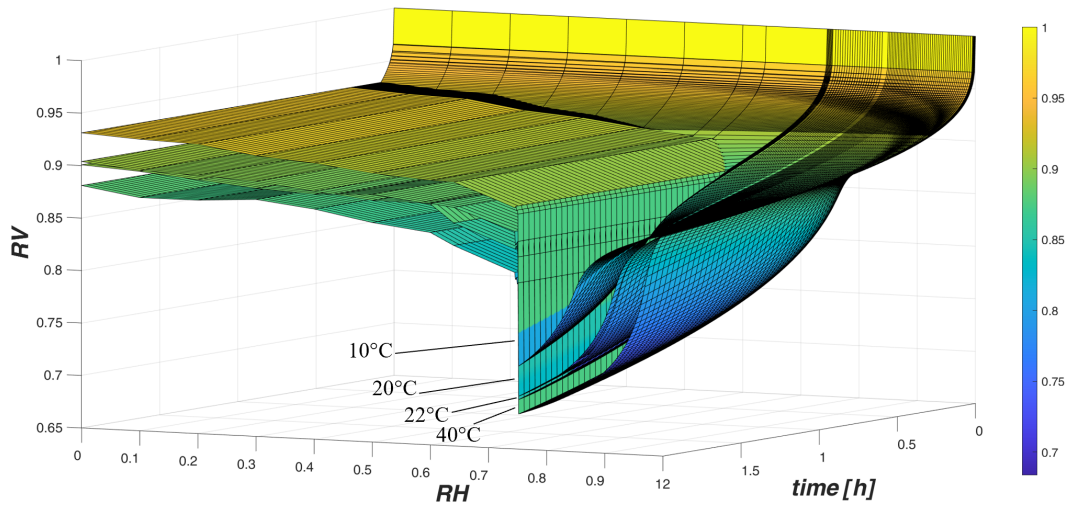


FIG. 12. Results of model calculations of the evaporation process of a sessile droplet of aqueous solution in terms of relative viability, RV , of the MS2 virus as a function of the time and the RH at $T = 10, 20, 22,$ and 40°C (calculations refer to the case $V_{mix0} = 1\ \mu\text{l}$, $c_{s0} = 10\ \text{kg/m}^3$, and $\theta_0 = 86^\circ$).

T) and (ii) an increasing trend of RV with increasing temperature. We recall that a power law function was used, Eq. (30), to define a realistic analytical relationship between RV and CD to be used in our simulations. When the droplet is in regime I, Eq. (10), it has been observed that it undergoes water condensation from the air, and the salt concentration within the droplet decreases with a consequent reduced value of the integral over time of the salt concentration, Eq. (29). According to Eq. (30), this occurrence leads to a RV always approaching the value of 1 during the evaporation process. Conversely, when the droplet is in regime II, Eq. (11), a continuous decreasing RH leads to progressively faster evaporation process and, therefore, to greater final values of salt concentration when the equilibrium is established. This occurrence translates into greater values of CD and then the transition in a region when the RV is strongly reduced, Eq. (30). This transition generates the U-shaped curve observed for the virus viability. Finally, as for regime III, Eq. (12), it is again expected that water evaporates from the droplet and that the volume decreases, while the salt concentration increases, reaching its saturation value, and complete evaporation is attained. In this case, the complete evaporation does not allow to obtain high values of CD and, therefore, the RV dramatically increases again to a value of 1, Eq. (30). This occurrence determines the discontinuous transition from the U-shape behavior to a rather flattened RV . Indeed, at RH values falling within the regime III region, the droplet completely evaporates before a harmful CD is attained and the virus survives as it is no longer encapsulated into a highly concentrated solution.⁴¹

We underline that our simulations are based on Eq. (30), which is intended to relate RV to CD at 22°C . Hence, the behaviors predicted at temperature values lower or higher than 22°C do account only for the physical effect of temperature on the evolution of the droplet and, in turn, of salt concentration, that is, an indirect effect of temperature on the RV of the virus. Actually, we disregard a possible direct effect of temperature on the relative viability of the virus consisting in the temperature dependence of the fitting parameters in Eq. (30), which we can refer to as an “intrinsic” temperature effect on the relative viability

of the virus. This approximation would likely promote an underestimation of the survival capability of the virus at temperature values below 22°C . If experimental evidence were available, model parameters in Eq. (30) should be then properly modified to account for this important temperature effect for making quantitative theoretical predictions.

Unfortunately, there are no data available in the literature in a form that allows a meaningful comparison with the theoretical results of the proposed model. Recently, Prussin *et al.*¹⁹ have reported some interesting experimental results referring to the Phi6 virus, which represents a suitable surrogate of coronavirus. In this work, the authors investigated the infectivity of the Phi6 virus at four different temperatures ($14, 19, 25,$ and 37°C), reporting the “Relative infectious ratio”—calculated as N_E/N_C , where N_E and N_C are, respectively, the measured Phi6 concentrations for the exposed and control samples—as a function of RH and T . The virus infectivity was assessed by plaque forming units with $1\ \mu\text{l}$ of droplets (prepared stock solutions of virus by suspending propagated Phi6 in tryptic soy broth) on cell. After 2 h of incubation, it was observed that the highest Phi6 infectivity was at the lowest tested temperature (14°C), and there was a reduction in infectivity of more than 6-log when the temperature increased to 37°C as well. Although no direct comparison can be made between theoretical predictions illustrated in the present work and the results on Phi6, we note, however, that also the experimental results reported by Prussin *et al.*¹⁹ (curves at 25 and 37°C) display a U-shaped virus vitality as a function of RH .

IV. CONCLUSIONS

In this study, a quasi-steady diffusion-controlled evaporation model is extended to elucidate the evolution of aqueous sessile droplets containing viruses, resting on a flat smooth surface, and, from that, predict the viability of viruses.

The model rests on simple relations that allow a global analysis of the wetting regime on different substrates and the prediction of the

evaporation process at different ambient temperatures of droplets of aqueous sodium chloride solutions assumed as simulant of saliva.

We first investigated the evaporation behavior of the droplet when located on hydrophilic or hydrophobic surfaces, accounting for the different wetting regimes. The results revealed that in the case of CCR (*constant contact radius*, associated with hydrophilic surfaces) condition, the evaporation time increases with the initial contact angle, while in the case of CCA (*constant contact angle*, attributed to hydrophobic surfaces) condition, the evaporation time exhibits an opposite trend. In the case of the SS (*stick-slip*) condition, it is shown that the evaporation time increases with both the initial and the receding contact angles, emphasizing that CCR and CCA represent the extreme cases of this third wetting behavior.

Then, we analyzed the different evaporation regimes that may arise depending on the selected ambient conditions. It has been shown that the sessile droplet displays longer evaporation times at low temperature and high humidity conditions, highlighting the importance of the latter in the occurrence of salt crystallization and precipitation.

Although saliva droplets are characterized by a complex mixture of several salts (including the sodium chloride), proteins, surfactants, and some other nonvolatile components, we assumed that the sodium chloride aqueous solution could account for a virus-laden sessile droplet, as we considered the salt concentration for being the discriminant for the virus viability, as already reported in the literature. In this way, it was possible to build interconnected charts of evaporation time and relative viability related to the survival of MS2 virus, considered to be a surrogate of the SARS-CoV-2. It was observed that the virus exhibits a higher mortality when the surface, on which the droplet is located, is characterized by a CCR regime or, at least, a SS regime approaching the CCR. Regarding the effect of RH and temperature, the model predicts that the relative viability of the MS2 virus exhibits a U-shape as a function of the relative humidity, with a viability that increases with temperature when at low humidity. Notably, a similar U-shaped behavior of the relative Infectious Ratio vs RH has also been recently found experimentally and reported in the literature for Phi6, an encapsulated virus, contained in droplets exposed to environments at different temperatures and RHs.

The developed model presents some limitations that will be addressed in future studies, such as the interaction between the sessile droplet and complex substrates (e.g., surfaces with certain topographical features and/or chemical heterogeneity), the complex composition of the saliva droplets (e.g., the presence of also proteins, surfactants, and some other nonvolatile compounds), and the interaction among multiple droplets that would occur in the case of a cloud that is expelled from mouth and/or nose and that deposit on the surface. Moreover, due to the lack of experimental information, the model, in the form presented in this contribution, disregards possible intrinsic temperature effect on the relative viability of a virus, potentially leading to underestimated values of the RV from theoretical simulations at low temperature (below 20 °C).

ACKNOWLEDGMENTS

C.B. was supported by the University of Trento within the Project COVID 2021 ACOV-SURF. N.M.P. and M.F. were supported by the Italian Ministry of Education, University and Research (MIUR) under the PRIN-20177TTP3S grant.

AUTHOR DECLARATIONS

Conflict of Interest

The authors have no conflicts to disclose.

Author Contributions

Cosimo Brondi: Data curation (equal); Investigation (equal). **Nicola Giuseppe Di Novo:** Data curation (equal); Investigation (equal). **Nicola M. Pugno:** Conceptualization (equal). **Giuseppe Mensitieri:** Conceptualization (equal); Writing – original draft (equal); Writing – review & editing (equal). **Massimiliano Fraldi:** Conceptualization (equal); Writing – original draft (equal); Writing – review & editing (equal).

DATA AVAILABILITY

The data that support the findings of this study are available from the corresponding authors upon reasonable request.

REFERENCES

1. J. Lazarus, "A multinational Delphi consensus to end the COVID-19 public health threat," *Nature* **611**, 332–345 (2022).
2. T. Dbouk and D. Drikakis, "On coughing and airborne droplet transmission to humans," *Phys. Fluids* **32**, 053310 (2020).
3. M. R. Pendar and J. C. Páscoa, "Numerical modeling of the distribution of virus carrying saliva droplets during sneeze and cough," *Phys. Fluids* **32**, 083305 (2020).
4. L. M. Casanova, S. Jeon, W. A. Rutala, D. J. Weber, and M. D. Sobsey, "Effects of air temperature and relative humidity on coronavirus survival on surfaces," *Appl. Environ. Microbiol.* **76**, 2712–2717 (2010).
5. S. David, K. Sefiane, and L. Tadrist, "Experimental investigation of the effect of thermal properties of the substrate in the wetting and evaporation of sessile drops," *Colloids Surf., A* **298**, 108–114 (2007).
6. S. Semenov, V. M. Starov, R. G. Rubio, and M. G. Velarde, "Instantaneous distribution of fluxes in the course of evaporation of sessile liquid droplets: Computer simulations," *Colloids Surf., A* **372**, 127–134 (2010).
7. A. J. D. Shaikeea and S. Basu, "Evaporating sessile droplet pair: Insights into contact line motion, flow transitions and emergence of universal vaporisation pattern," *Appl. Phys. Lett.* **108**, 244102 (2016).
8. T. A. H. Nguyen, A. V. Nguyen, M. A. Hampton, Z. P. Xu, L. Huang, and V. Rudolph, "Theoretical and experimental analysis of droplet evaporation on solid surfaces," *Chem. Eng. Sci.* **69**, 522–529 (2012).
9. H. Matsui, Y. Noda, and T. Hasegawa, "Hybrid energy-minimization simulation of equilibrium droplet shapes on hydrophilic/hydrophobic patterned surfaces," *Langmuir* **28**, 15450–15453 (2012).
10. X. Zhong, J. Ren, K. S. Chong, K. Ong, and F. Duan, "Wetting transition at a threshold surfactant concentration of evaporating sessile droplets on a patterned surface," *Langmuir* **35**, 4509–4517 (2019).
11. J. Fukai, H. Ishizuka, Y. Sakai, M. Kaneda, M. Morita, and A. Takahara, "Effects of droplet size and solute concentration on drying process of polymer solution droplets deposited on homogeneous surfaces," *Int. J. Heat Mass Transfer* **49**, 3561–3567 (2006).
12. L. K. Malla, R. Bhardwaj, and A. Neild, "Analysis of profile and morphology of colloidal deposits obtained from evaporating sessile droplets," *Colloids Surf., A* **567**, 150–160 (2019).
13. S. Semenov, A. Trybala, R. G. Rubio, N. Kovalchuk, V. Starov, and M. G. Velarde, "Simultaneous spreading and evaporation: Recent developments," *Adv. Colloid Interface Sci.* **206**, 382–398 (2014).
14. K. Sefiane, "The coupling between evaporation and adsorbed surfactant accumulation and its effect on the wetting and spreading behaviour of volatile drops on a hot surface," *J. Pet. Sci. Eng.* **51**, 238–252 (2006).
15. E. F. Crafton and W. Z. Black, "Heat transfer and evaporation rates of small liquid droplets on heated horizontal surfaces," *Int. J. Heat Mass Transfer* **47**, 1187–1200 (2004).

- ¹⁶F. Girard, M. Antoni, S. Faure, and A. Steinchen, "Influence of heating temperature and relative humidity in the evaporation of pinned droplets," *Colloids Surf., A* **323**, 36–49 (2008).
- ¹⁷W. Yang, S. Elankumaran, and L. C. Marr, "Relationship between humidity and influenza A viability in droplets and implications for influenza's seasonality," *PLoS One* **7**, e46789 (2012).
- ¹⁸W. Yang and L. C. Marr, "Mechanisms by which ambient humidity may affect viruses in aerosols," *Appl. Environ. Microbiol.* **78**, 6781–6788 (2012).
- ¹⁹A. J. Prussin, D. O. Schwake, K. Lin, D. L. Gallagher, L. Buttlng, and L. C. Marr, "Survival of the enveloped virus Phi6 in droplets as a function of relative humidity, absolute humidity, and temperature," *Appl. Environ. Microbiol.* **84**, e00551 (2018).
- ²⁰K. Lin and L. C. Marr, "Humidity-dependent decay of viruses, but not bacteria, in aerosols and droplets follows disinfection kinetics," *Environ. Sci. Technol.* **54**, 1024–1032 (2020).
- ²¹R. Bhardwaj and A. Agrawal, "Likelihood of survival of coronavirus in a respiratory droplet deposited on a solid surface," *Phys. Fluids* **32**, 061704 (2020).
- ²²R. Bhardwaj and A. Agrawal, "How coronavirus survives for days on surfaces," *Phys. Fluids* **32**, 111706 (2020).
- ²³S. Kumar, "Insight on the evaporation dynamics in reducing the COVID-19 infection triggered by respiratory droplets," *Phys. Fluids* **33**, 072004 (2021).
- ²⁴D. Hu and H. Wu, "Volume evolution of small sessile droplets evaporating in stick-slip mode," *Phys. Rev. E* **93**, 042805 (2016).
- ²⁵N. G. Di Novo, A. R. Carotenuto, G. Mensitieri, M. Fraldi, and N. M. Pugno, "Modeling of virus survival time in respiratory droplets on surfaces: A new rational approach for antiviral strategies," *Front. Mater.* **8**, 631723 (2021).
- ²⁶H. Hu and R. G. Larson, "Evaporation of a sessile droplet on a substrate," *J. Phys. Chem. B* **106**, 1334–1344 (2002).
- ²⁷Y. O. Popov, "Evaporative deposition patterns: Spatial dimensions of the deposit," *Phys. Rev. E* **71**, 036313 (2005).
- ²⁸E. L. Talbot, A. Berson, P. S. Brown, and C. D. Bain, "Evaporation of picoliter droplets on surfaces with a range of wettabilities and thermal conductivities," *Phys. Rev. E* **85**, 061604 (2012).
- ²⁹A. M. Cazabat and G. Guéna, "Evaporation of macroscopic sessile droplets," *Soft Matter* **6**, 2591–2612 (2010).
- ³⁰R. G. Picknett and R. Bexon, "The evaporation of sessile or pendant drops in still air," *J. Colloid Interface Sci.* **61**, 336–350 (1977).
- ³¹C. Bourges-Monnier and M. E. R. Shanahan, "Influence of evaporation on contact angle," *Langmuir* **11**, 2820–2829 (1995).
- ³²D. L. Nuding, E. G. Rivera-Valentin, R. D. Davis, R. V. Gough, V. F. Chevrier, and M. A. Tolbertad, "Deliquescence and efflorescence of calcium perchlorate: An investigation of stable aqueous solutions relevant to Mars," *Icarus* **243**, 420–428 (2014).
- ³³K. S. Pitzer, J. C. Peiper, and R. H. Busey, "Thermodynamic properties of aqueous sodium chloride solutions," *J. Phys. Chem.* **13**, 1–102 (1984).
- ³⁴B. E. Poling, G. H. Thomson, D. G. Friend, R. L. Rowley, and W. V. Wilding, "Physical and chemical data," in *Perry's Chemical Engineers Handbook*, 8th ed. (McGraw Hill, 2005), Vol. 2, p. 110.
- ³⁵D. Bonn, J. Eggers, J. Indekeu, J. Meunier, and E. Rolley, "Wetting and spreading," *Rev. Mod. Phys.* **81**, 739 (2009).
- ³⁶M. E. R. Shanahan and A. Carre, "Viscoelastic dissipation in wetting and adhesion phenomena," *Langmuir* **11**, 1396–1402 (1995).
- ³⁷J. M. Stauber, S. K. Wilson, B. R. Duffy, and K. Sefiane, "On the lifetimes of evaporating droplets," *J. Fluid Mech.* **744**, R2 (2014).
- ³⁸D. H. Shin, S. H. Lee, J. Y. Jung, and J. Y. Yoo, "Evaporating characteristics of sessile droplet on hydrophobic and hydrophilic surfaces," *Microelectron. Eng.* **86**, 1350–1353 (2009).
- ³⁹V. Souliè, S. Karpitschka, F. Lequien, P. Prenè, T. Zemb, H. Moehwald, and H. Riegler, "The evaporation behavior of sessile droplets from aqueous saline solutions," *Phys. Chem. Chem. Phys.* **17**, 22296 (2015).
- ⁴⁰M. S. Hasan, K. Sobolev, and M. Nosonovsky, "Evaporation of droplets capable of bearing viruses airborne and on hydrophobic surfaces," *Phys. Fluids* **129**, 024703 (2021).
- ⁴¹H. Choi and C. D. Montemagno, "Assessment of osmotic characteristics of influenza viruses," in *Epidemiology—Research and Practice*, 1st ed. (iConcept Press Ltd., Hong Kong, China, 2014), p. 19.
- ⁴²A. Cordova, M. Deserno, W. M. Gelbart, and A. Ben-Shaul, "Osmotic shock and the strength of viral capsids," *Biophys. J.* **85**, 70–74 (2003).
- ⁴³E. Huynh, A. Olinger, D. Woolley, R. K. Kohli, J. M. Choczynski, J. F. Davies, K. Lin, L. C. Marr, and R. D. Davis, "Evidence for a semisolid phase state of aerosols and droplets relevant to the airborne and surface survival of pathogens," *Proc. Natl. Acad. Sci. U.S.A.* **119**, e2109750119 (2022).
- ⁴⁴C. E. Rowell and H. M. Dobrovolny, "Energy requirements for loss of viral infectivity," *Food Environ. Virol.* **12**, 281–294 (2020).
- ⁴⁵D. H. Morris, K. C. Yinda, A. Gamble, F. W. Rossine, Q. Huang, T. Bushmaker, R. J. Fischer, M. J. Matson, N. Van Doremalen, P. J. Vikesland, L. C. Marr, V. J. Munster, and J. O. Lloyd-Smith, "Mechanistic theory predicts the effects of temperature and humidity on inactivation of SARS-CoV-2 and other enveloped viruses," *eLife* **10**, e65902 (2021).
- ⁴⁶H. A. Aboubakr, T. A. Sharafeldin, and S. M. Goyal, "Stability of SARS-CoV-2 and other coronaviruses in the environment and on common touch surfaces and the influence of climatic conditions: A review," *Transboundary Emerging Dis.* **68**, 296–312 (2020).
- ⁴⁷A. W. H. Chin, J. T. S. Chu, M. R. A. Perera, K. P. Y. Hui, H. Yen, M. C. W. Chan, M. Peiris, and L. L. M. Poon, "Stability of SARS-CoV-2 in different environmental conditions," *Lancet Microbe* **1**, e10 (2020).
- ⁴⁸Y. Li, J. Q. Pham, K. P. Johnston, and P. F. Green, "Contact angle of water on polystyrene thin films: Effects of CO₂ environment and film thickness," *Langmuir* **23**, 9785–9793 (2007).